nature physics

ARTICLES

https://doi.org/10.1038/s41567-018-0134-8

Corrected: Publisher Correction

Pressure tuning of light-induced superconductivity in K_3C_{60}

A. Cantaluppi[1,2,6], M. Buzzi[1,6], G. Jotzu[1], D. Nicoletti[1,2], M. Mitrano[1], D. Pontiroli[3], M. Riccò[3], A. Perucchi[4], P. Di Pietro[4] and A. Cavalleri[1,2,5*]

Optical excitation at terahertz frequencies has emerged as an effective means to dynamically manipulate complex materials. In the molecular solid K_3C_{60}, short mid-infrared pulses transform the high-temperature metal into a non-equilibrium state with the optical properties of a superconductor. Here we tune this effect with hydrostatic pressure and find that the superconducting-like features gradually disappear at around 0.3 GPa. Reduction with pressure underscores the similarity with the equilibrium superconducting phase of K_3C_{60}, in which a larger electronic bandwidth induced by pressure is also detrimental for pairing. Crucially, our observation excludes alternative interpretations based on a high-mobility metallic phase. The pressure dependence also suggests that transient, incipient superconductivity occurs far above the 150 K hypothesized previously, and rather extends all the way to room temperature.

Resonant optical excitation of infrared-active phonon modes can drive the crystal lattice of solids nonlinearly[1], excite other orders coherently[2], switch lattice polarization[3], drive insulator-to-metal[4] or magnetic transitions[5], and even induce transient superconductivity above equilibrium T_c[6,7]. In the potassium-doped fulleride K_3C_{60}, a superconductor with critical temperature $T_c = 20$ K, excitation of local molecular vibrations was shown to induce superconducting-like optical properties in the high-temperature metal ($T > T_c$)[8]. Key features of this state are a 12 meV wide gap in the frequency-dependent optical conductivity $\sigma_1(\omega)$, twice as large as the equilibrium 6 meV wide superconducting gap, and a divergent low-frequency imaginary conductivity $\sigma_2(\omega)$, indicative of high carrier mobility. This state was found to extend to at least 100 K, hence up to temperature scales far in excess of equilibrium T_c (20 K). For $T > 100$ K, a partially gapped state was reported. In this higher-temperature regime, the light-induced state can be interpreted either as a high-mobility metal en route to a transient superconducting state, or as an incipient superconductor, which is only partially coherent.

Many theoretical mechanisms have been invoked to explain these observations, ranging from a dynamical reduction of the electronic bandwidth[9] to the parametric amplification of the pairing instability[10] and to electron attraction[11] in vibrationally excited molecular sites[12,13]. Recent experiments in bilayer graphene are consistent with some of these suggestions[9,10], as the optical excitation of a vibrational mode similar to that driven in K_3C_{60} appears to increase the electron–phonon interaction[14]. Finally, recent theoretical work has raised the possibility that photostimulation may involve optical excitation and cooling of above-gap thermal quasiparticles into a superexcitonic state with high electronic heat capacity[15].

The face-centred cubic structure of doped fullerides A_3C_{60} is shown in Fig. 1a. Three electrons are donated by the alkali atoms to each C_{60} molecule, which then form three narrow, half-filled bands near the Fermi level. Figure 1c shows how the equilibrium superconducting transition appears in the steady-state optical properties of K_3C_{60}, measured above and below $T_c = 20$ K. When cooling metallic K_3C_{60} (red curves) below T_c, one observes large changes in the optical properties: a saturation of the low-frequency reflectivity to $R = 1$, a 6 meV gap in the real part of the optical conductivity $\sigma_1(\omega)$, and a $1/\omega$ divergence in the imaginary part $\sigma_2(\omega)$[8,16] (blue curves).

As superconductivity in K_3C_{60} emerges from a combination of Jahn–Teller intramolecular distortions and electronic correlations[17–19], it is natural to explore the response of the material to direct excitation of optically accessible vibrational modes. In Fig. 1d we report the optical properties of polycrystalline powders of K_3C_{60}, 1 ps after the excitation tuned to 'on-ball' infrared-active modes of T_{1u} symmetry at 170 meV energy (7.3 μm wavelength), whose atomic distortion is displayed in Fig. 1b. At this frequency, strongly correlated metallic carriers are also excited, as the radiation is also resonant with a broad absorption peak extending from about 40 to 200 meV[20], whose precise origin is still unclear[15]. A broadband probe pulse was used to detect the light-induced changes in the optical reflectivity and complex optical conductivity between 1.6 and 7 THz (6.5–29 meV) using THz time-domain spectroscopy. Starting from the unperturbed metallic state at 100 K (red curves), we observed an increase in the reflectivity, which saturates to $R = 1$ for all probe photon energies below 12 meV, a gapped $\sigma_1(\omega)$ and a divergent $\sigma_2(\omega)$. These data confirm the results of ref. [8], but were recorded with an improved apparatus, involving higher pump fluence and a broader probe bandwidth (see Supplementary Information S3).

In this paper, we study how the features reported in Fig. 1d change with the application of hydrostatic pressure. At equilibrium, the application of pressure reduces the superconducting transition temperature T_c, because of the increase in the electronic bandwidth when the intermolecular spacing is reduced[21,22]. As shown in Fig. 2, the size of the optical gap ($2\Delta_0$) and the critical temperature[23,24] decay linearly even at relatively modest pressures. Due to the low bulk modulus (28 GPa; ref. [24]), a pressure of 3 GPa reduces the superconducting gap to less than half of the ambient-pressure value, as the electronic bandwidth increases by about 25% (ref. [25]).

[1]Max Planck Institute for the Structure and Dynamics of Matter, Hamburg, Germany. [2]The Hamburg Centre for Ultrafast Imaging, Hamburg, Germany. [3]Dipartimento di Scienze Matematiche, Fisiche e Informatiche, Università degli Studi di Parma, Parma, Italy. [4]INSTM UdR Trieste-ST and Elettra-Sincrotrone Trieste, Trieste, Italy. [5]Department of Physics, Oxford University, Clarendon Laboratory, Oxford, UK. [6]These authors contributed equally: A. Cantaluppi, M. Buzzi. *e-mail: andrea.cavalleri@mpsd.mpg.de

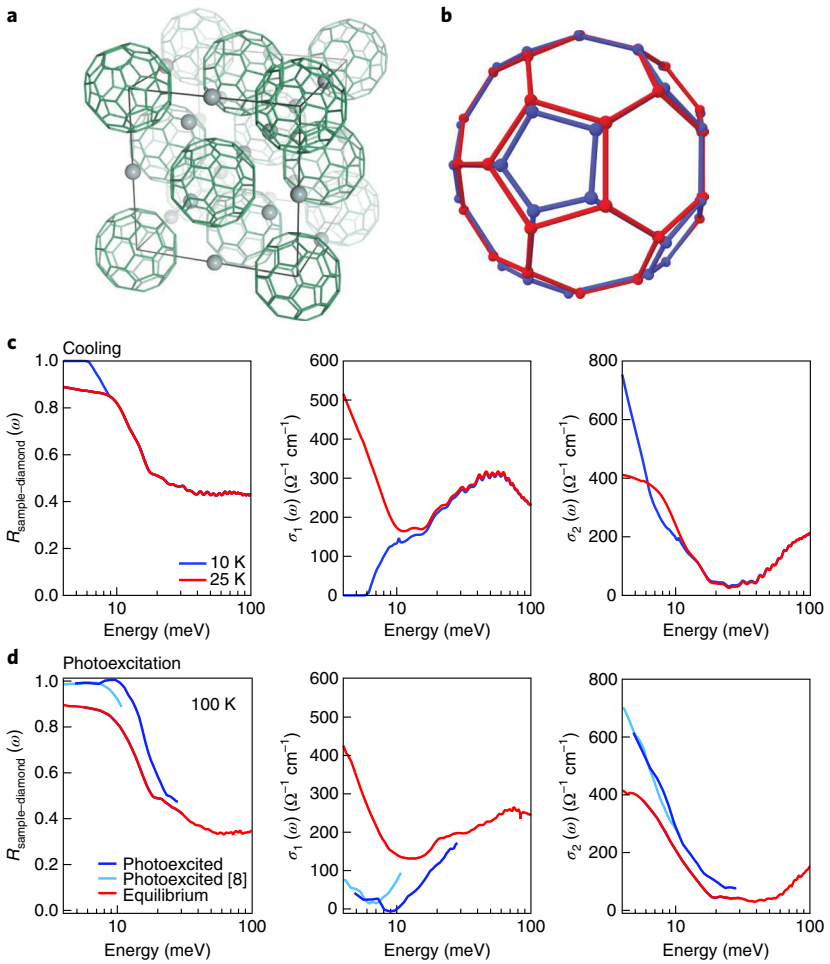

Fig. 1 | Structure, equilibrium phase transition, and transient light-induced phase of K_3C_{60}. **a**, The fcc crystal structure of K_3C_{60} (ref. [28]). The C_{60} molecules are represented by the green bonds connecting all the C atoms. The grey spheres are the K atoms, acting as spacers between neighbouring buckyballs. The equilibrium lattice constant is 14.26 Å at room temperature. **b**, C_{60} molecular distortion (blue) along the $T_{1u}(4)$ vibrational mode coordinates. The equilibrium structure is shown in red. **c**, Reflectivity (sample–diamond interface) and real and imaginary optical conductivity—$R(\omega)$, $\sigma_1(\omega)$ and $\sigma_2(\omega)$—across the equilibrium superconducting transition in K_3C_{60}. The red curves are measured at 25 K, in the metallic phase. The blue curves refer to the equilibrium superconductor (10 K). **d**, Reflectivity (sample–diamond interface) and real and imaginary optical conductivity—$R(\omega)$, $\sigma_1(\omega)$ and $\sigma_2(\omega)$—of K_3C_{60} at equilibrium (red) and 1 ps after photoexcitation (blue) at $T = 100$ K. The light-blue curves show the data reported in ref. [8], measured with a fluence of 1 mJ cm^{-2}, while those in dark blue were measured with a broader probe spectrum and a higher pump fluence (3 mJ cm^{-2}).

Figure 3 displays snapshots of the measured optical reflectivity $R(\omega)$ at the sample–diamond interface, along with complex conductivity spectra, $\sigma_1(\omega)$ and $\sigma_2(\omega)$, for different values of static pressure. The exact pressure was measured with calibrated ruby fluorescence (see Supplementary Information S3). In each panel, the red and blue curves trace the optical properties of the equilibrium metal and those of the non-equilibrium state induced by photoexcitation, respectively. For pressures up to 0.17 GPa (Fig. 3a-c) the transient optical response of K_3C_{60} is similar to that observed at ambient pressure, with a reflectivity approaching $R = 1$, a gapped $\sigma_1(\omega)$ and a divergent $\sigma_2(\omega)$ toward low frequencies. However, some spectral weight is also found in $\sigma_1(\omega)$ at low energies, indicative of reduced coherence.

As the applied pressure increases, a stronger suppression of the light-induced changes in both the reflectivity and complex optical conductivity is observed (Fig. 3d,e). Above 0.3 GPa the enhancement in the reflectivity is clearly less pronounced, and a progressively broader Drude peak appears at low frequency in the $\sigma_1(\omega)$ spectrum.

The reduction in light-induced coherence observed as a function of pressure is clearly not compatible with the behaviour expected for

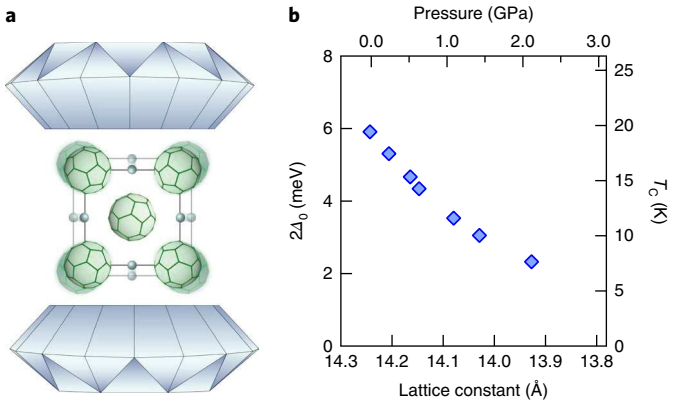

Fig. 2 | Equilibrium pressure dependence of superconducting K_3C_{60}. **a**, Schematic representation of a diamond anvil cell on the K_3C_{60} crystal structure. By applying external pressure, the intermolecular distances are reduced. **b**, Superconducting transition temperature and calculated optical gap ($2\Delta_0/k_BT = 3.52$; ref. [23]), plotted as a function of lattice parameter and external pressure. Data adapted from refs [24,29].

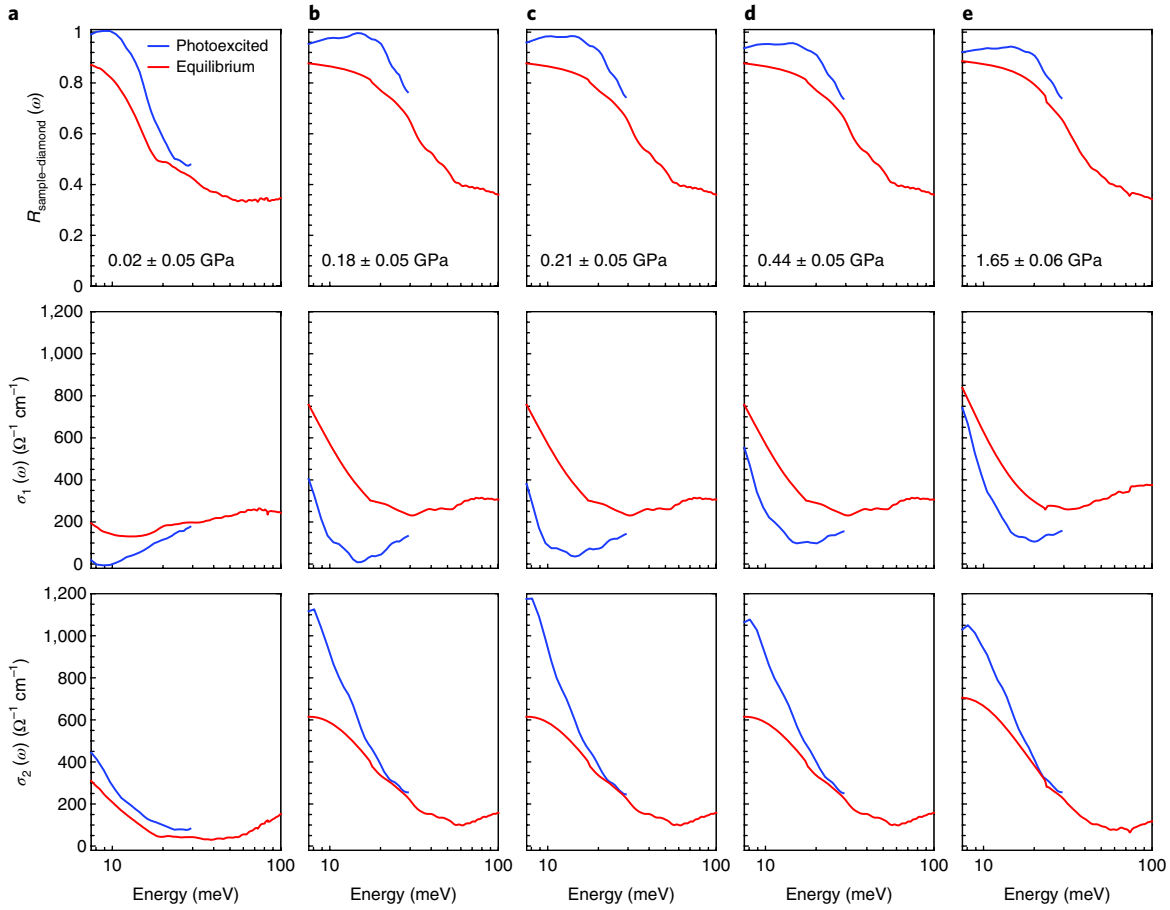

Fig. 3 | Pressure dependence of the transient optical properties of K_3C_{60} at $T = 100$ K. Reflectivity (sample–diamond interface) and complex optical conductivity of K_3C_{60} measured at equilibrium and 1 ps after photoexcitation at $T = 100$ K, for different external hydrostatic pressures. All data were taken with the same pump fluence of 3 mJ cm^{-2}.

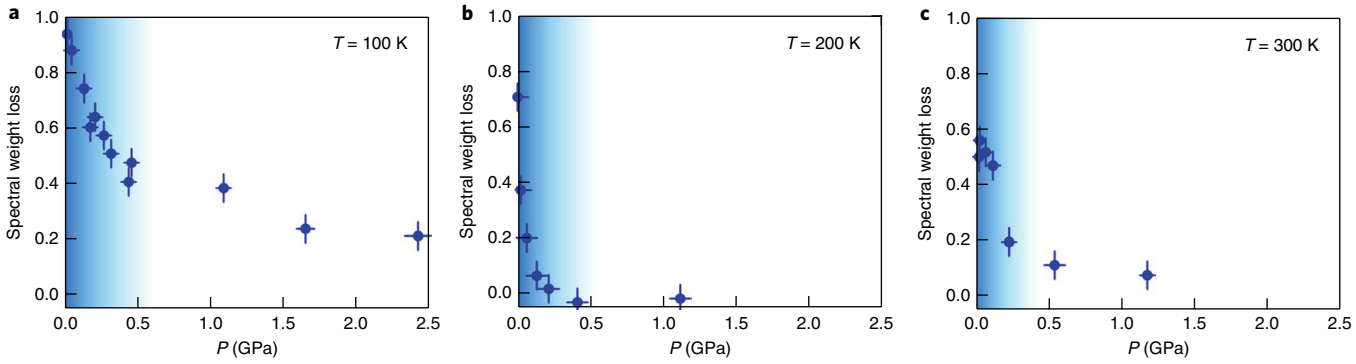

Fig. 4 | Scaling of the $\sigma_1(\omega)$ gap with external pressure. Photoinduced reduction in $\sigma_1(\omega)$ spectral weight, integrated between 6.5 and 12.9 meV, normalized by the equilibrium value (integrated in the same range). The blue shaded areas identify the regions in which a photoinduced conductivity gapping is measured. All data were taken with the same pump fluence (3 mJ cm^{-2}). Vertical error bars represent uncertainties determined from different sets of measurements and horizontal error bars show the calibration uncertainty of the ruby fluorescence measurements used to determine the pressure (see Supplementary Information S3).

a light-induced metallic state, as a lattice compression in a metal is typically associated with larger electronic bandwidth, smaller effective mass and higher mobility. This is for example evident when analysing the equilibrium metallic properties in the red curves of Fig. 3 (see also Supplementary Information S2), where we observe higher plasma frequencies ω_p with increasing pressure.

In Fig. 4 we report the fractional spectral weight loss for frequencies inside the gapped region of the spectrum, obtained by integrating $\sigma_1(\omega)$ between 6.5 and 12.9 meV for different pressures and base temperatures of 100 K, 200 K and 300 K (see Supplementary Information S9 for full data sets at 200 and 300 K). Shaded blue areas indicate the pressure–temperature ranges where the light-

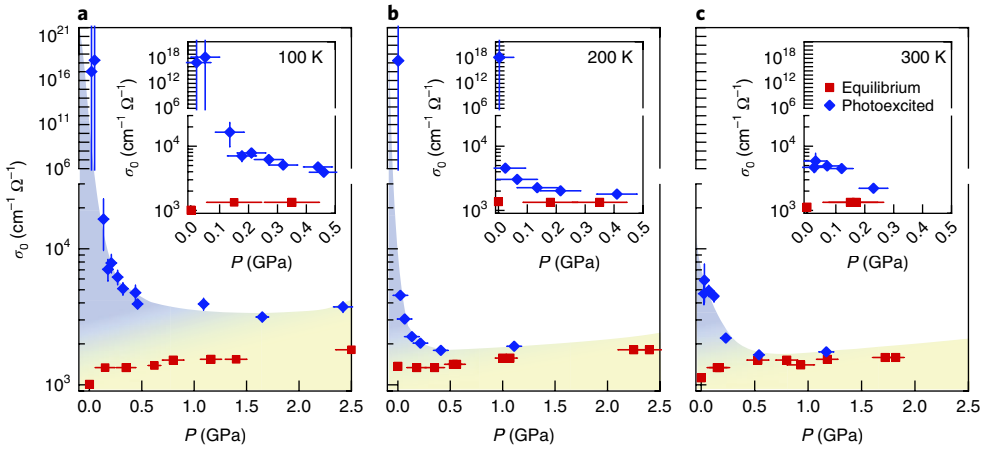

Fig. 5 | Pressure dependence of the extrapolated conductivity. Blue diamonds are extrapolated zero-frequency conductivities extracted from Drude–Lorentz fits of the transient optical spectra, as a function of pressure and for three different temperatures: 100 K (**a**), 200 K (**b**) and 300 K (**c**). Red squares are the corresponding zero-frequency conductivities determined at equilibrium. The blue areas identify the regions in which σ_0 is suppressed by pressure ($d\sigma_0/dP<0$) while those in yellow indicate the regime in which $d\sigma_0/dP>0$. All data were taken with the same pump fluence (3 mJ cm^{-2}). The insets show a close-up of the low-pressure region. Vertical error bars reflect the fit uncertainty and horizontal error bars show the calibration uncertainty of the ruby fluorescence measurements used to determine the pressure (see Supplementary Information S3).

induced state is gapped. Overall, the light-induced gap fills even at moderate pressure values, becoming even smaller for increasing temperature. For $P\gtrsim 0.3$ GPa, the pressure dependence of the light-induced effects is strongly reduced.

Fits to the optical properties of Fig. 3 make the qualitative analysis above quantitatively significant (see Supplementary Information S10). By fitting the transient optical response of K_3C_{60}, we extrapolated the value of the low-frequency optical conductivity $\sigma_0=\lim_{\omega\to 0}\sigma_1(\omega)$. To compare both superconducting-like and metallic-like states in a consistent fashion, we used a Drude–Lorentz fit for the entire pressure range, in which σ_0 was allowed to float from finite (metal) to infinite values (perfect conductor), and a single lorentzian was used to capture the mid-infrared absorption band extending from 40 to 200 meV.

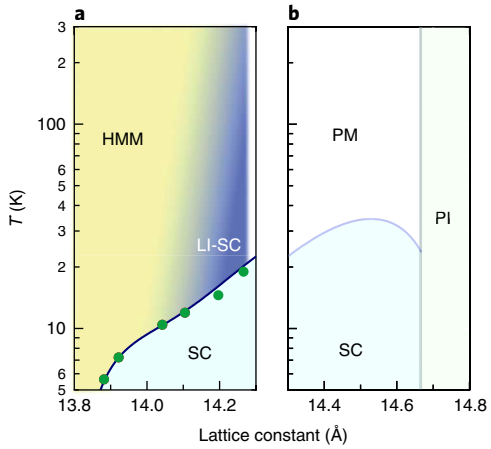

Fig. 6 | Out-of-equilibrium phase diagram of fcc K_3C_{60}. a, K_3C_{60} phase diagram (T versus room-temperature lattice constant and pressure). Green filled circles indicate the superconducting transition temperature (T_c) measured for different lattice parameters[24] at equilibrium. The light-blue filled area defines the equilibrium superconducting phase (SC). The dark-blue shading stands for the light-induced superconductor (LI-SC), which evolves into a high-mobility metal (HMM) under the application of pressure (yellow area). **b**, Extension of the fcc A_3C_{60} phase diagram for larger lattice constants. PI, PM and SC refer to the equilibrium paramagnetic insulating, paramagnetic metallic and superconducting phases, respectively. Based on refs [17,28,29].

The results of this analysis are summarized in Fig. 5, where we report the pressure dependence of σ_0 for three temperatures (100 K, 200 K, and 300 K). The red squares refer to the equilibrium metal, while the blue diamonds to the photoexcited state. As shown in these plots, the equilibrium metallic conductivity increases with applied pressure. In contrast, two pressure regimes are found for the light-induced state, one in which σ_0 decreases for small pressures ($d\sigma_0/dP<0$, blue shaded area) and one where it eventually increases slightly for higher pressures ($d\sigma_0/dP>0$, yellow shaded area). Several indications can be extracted from these data.

First, as mentioned above, from the optical properties alone reported in ref. [8], one could not uniquely differentiate a superconductor from a perfect conductor, as optics only identifies the density of charge carriers and the scattering rate. The hydrostatic pressure dependence reported here adds crucial information. At low pressures, the photoexcited state has clear superconducting-like pressure dependence ($d\sigma_0/dP<0$), whereas for higher pressures the response is clearly metal-like ($d\sigma_0/dP>0$). Furthermore, at high pressures the σ_0 of the photoexcited state follows the same slope as that of the equilibrium metal.

In this context the results reported for high temperatures ($T=200$ K and $T=300$ K) are surprising. In this temperature range, a high-mobility metallic state was proposed to interpret the data of ref. [8]. However, this interpretation was also not unique, as a superconducting-like state with progressively lower coherence could also have explained the data. Figure 5 suggests that in the low-pressure regime the $d\sigma_0/dP<0$ behaviour is retained all the way to 300 K, suggesting that some incipient features of transient superconductivity may already be present up to room temperature.

These observations also provide guidance for a microscopic explanation of our results. Indeed, as summarized in Fig. 6, we find a very strong dependence of the light-induced optical conductivity on pressure, and for the higher-pressure ranges (smaller lattice constants) the metallic phase (yellow) is stabilized. Our data set

an important benchmark for theories of photoinduced superconductivity[9–11,15,26,27], which should reproduce the observed pressure dependence. Figure 6 also indicates a clear path for future research in the broader context of A_3C_{60} superconductivity, showing on the right-hand side the region of the phase diagram still to be accessed (b), with the interesting perspective of optimizing light-induced superconductivity further, for even larger lattice spacing.

Data availability. The data sets generated and analysed during the current study are available from the corresponding author on reasonable request.

Received: 15 May 2017; Accepted: 6 April 2018;
Published online: 7 May 2018

References

1. Först, M. et al. Nonlinear phononics as an ultrafast route to lattice control. *Nat. Phys.* **7**, 854–856 (2011).
2. Nova, T. F. et al. An effective magnetic field from optically driven phonons. *Nat. Phys.* **13**, 132–136 (2017).
3. Mankowsky, R., von Hoegen, A., Först, M. & Cavalleri, A. Ultrafast reversal of the ferroelectric polarization. *Phys. Rev. Lett.* **118**, 197601 (2017).
4. Rini, M. et al. Control of the electronic phase of a manganite by mode-selective vibrational excitation. *Nature* **449**, 72–74 (2007).
5. Först, M. et al. Driving magnetic order in a manganite by ultrafast lattice excitation. *Phys. Rev. B* **84**, 241104(R) (2011).
6. Hu, W. et al. Optically enhanced coherent transport in $YBa_2Cu_3O_{6.5}$ by ultrafast redistribution of interlayer coupling. *Nat. Mater.* **13**, 705–711 (2014).
7. Mankowsky, R. et al. Nonlinear lattice dynamics as a basis for enhanced superconductivity in $YBa_2Cu_3O_{6.5}$. *Nature* **516**, 71–73 (2014).
8. Mitrano, M. et al. Possible light-induced superconductivity in K_3C_{60} at high temperature. *Nature* **530**, 461–464 (2016).
9. Coulthard, J. R., Clark, S. R., Al-Assam, S., Cavalleri, A. & Jaksch, D. Enhancement of superexchange pairing in the periodically driven Hubbard model. *Phys. Rev. B* **96**, 85104 (2017).
10. Knap, M., Babadi, M., Refael, G., Martin, I. & Demler, E. Dynamical Cooper pairing in nonequilibrium electron–phonon systems. *Phys. Rev. B* **94**, 214504 (2016).
11. Kennes, D. M., Wilner, E. Y., Reichman, D. R. & Millis, A. J. Transient superconductivity from electronic squeezing of optically pumped phonons. *Nat. Phys.* **13**, 479–483 (2017).
12. Kaiser, S. et al. Optical properties of a vibrationally modulated solid state Mott insulator. *Sci. Rep.* **4**, 3823 (2014).
13. Singla, R. et al. THz-frequency modulation of the Hubbard U in an organic Mott insulator. *Phys. Rev. Lett.* **115**, 187401 (2015).
14. Pomarico, E. et al. Enhanced electron–phonon coupling in graphene with periodically distorted lattice. *Phys. Rev. B* **95**, 24304 (2017).
15. Nava, A., Giannetti, C., Georges, A., Tosatti, E. & Fabrizio, M. Cooling quasiparticles in A_3C_{60} fullerides by excitonic mid-infrared absorption. *Nat. Phys.* **14**, 154–159 (2018).
16. Degiorgi, L., Briceno, G., Fuhrer, M. S., Zettl, A. & Wachter, P. Optical measurements of the superconducting gap in single-crystal K_3C_{60} and Rb_3C_{60}. *Nature* **369**, 541–543 (1994).
17. Nomura, Y., Sakai, S., Capone, M. & Arita, R. Unified understanding of superconductivity and Mott transition in alkali-doped fullerides from first principles. *Sci. Adv.* **1**, e1500568 (2015).
18. Capone, M., Fabrizio, M., Castellani, C. & Tosatti, E. Strongly correlated superconductivity. *Science* **296**, 2364–2366 (2002).
19. Gunnarsson, O. Superconductivity in fullerides. *Rev. Mod. Phys.* **69**, 575–606 (1997).
20. Degiorgi, L. et al. Optical properties of the alkali-metal-doped superconducting fullerenes: K_3C_{60} and Rb_3C_{60}. *Phys. Rev. B* **49**, 7012–7025 (1994).
21. Lorenz, B.. & Chu, C. W. in *Frontiers in Superconducting Materials* (ed. Narlikar, A. V.) 459–497 (Springer, Berlin, 2004).
22. Schilling, J. S. in *Handbook of High-Temperature Superconductivity* (ed. Schrieffer, J. R.) 427–462 (Springer, New York, NY, 2006).
23. Potočnik, A. et al. Size and symmetry of the superconducting gap in the f.c.c. Cs_3C_{60} polymorph close to the metal–Mott insulator boundary. *Sci. Rep.* **4**, 4265 (2015).
24. Zhou, O. et al. Compressibility of M_3C_{60} fullerene superconductors: relation between T_c and lattice parameter. *Science* **255**, 833–835 (1992).
25. Oshiyama, A. & Saito, S. Linear dependence of superconducting transition temperature on Fermi-level density-of-states in alkali-doped C_{60}. *Solid State Commun.* **82**, 41–45 (1992).
26. Kim, M. et al. Enhancing superconductivity in A_3C_{60} fullerides. *Phys. Rev. B* **94**, 155152 (2016).
27. Mazza, G. & Georges, A. Nonequilibrium superconductivity in driven alkali-doped fullerides. *Phys. Rev. B* **96**, 1–10 (2017).
28. Stephens, P. W. et al. Structure of single-phase superconducting K_3C_{60}. *Nature* **351**, 632–634 (1991).
29. Sparn, G. et al. Pressure dependence of superconductivity in single-phase K_3C_{60}. *Science* **252**, 1829–1831 (1991).

Acknowledgements

The research leading to these results received funding from the European Research Council under the European Union's Seventh Framework Programme (FP7/2007-2013)/ERC Grant Agreement 319286 (QMAC). We acknowledge support from the Deutsche Forschungsgemeinschaft via the excellence cluster The Hamburg Centre for Ultrafast Imaging—Structure, Dynamics and Control of Matter at the Atomic Scale and Priority Programme SFB925. M.B. acknowledges financial support from the Swiss National Science Foundation through an Early Postdoc Mobility Grant (P2BSP2_165352).

Author contributions

A. Cavalleri conceived the project together with M.M. and A. Cantaluppi. The time-resolved THz setup was built by A. Cantaluppi and M.B., who both made the pump–probe measurements and analysed the data with the support of G.J. and D.N. The equilibrium optical properties were measured by A. Cantaluppi and M.M., with the support of A.P. and P.D.P., and were then analysed by A. Cantaluppi and M.B. The samples were grown and characterized by D.P. and M.R. The manuscript was written by A. Cantaluppi, M.B., D.N. and A. Cavalleri, with input from all co-authors.

Competing financial interest

The authors declare no competing financial interests.

Additional information

Supplementary information is available for this paper at https://doi.org/10.1038/s41567-018-0134-8.

Reprints and permissions information is available at www.nature.com/reprints.

Correspondence and requests for materials should be addressed to A.C.

Publisher's note: Springer Nature remains neutral with regard to jurisdictional claims in published maps and institutional affiliations.